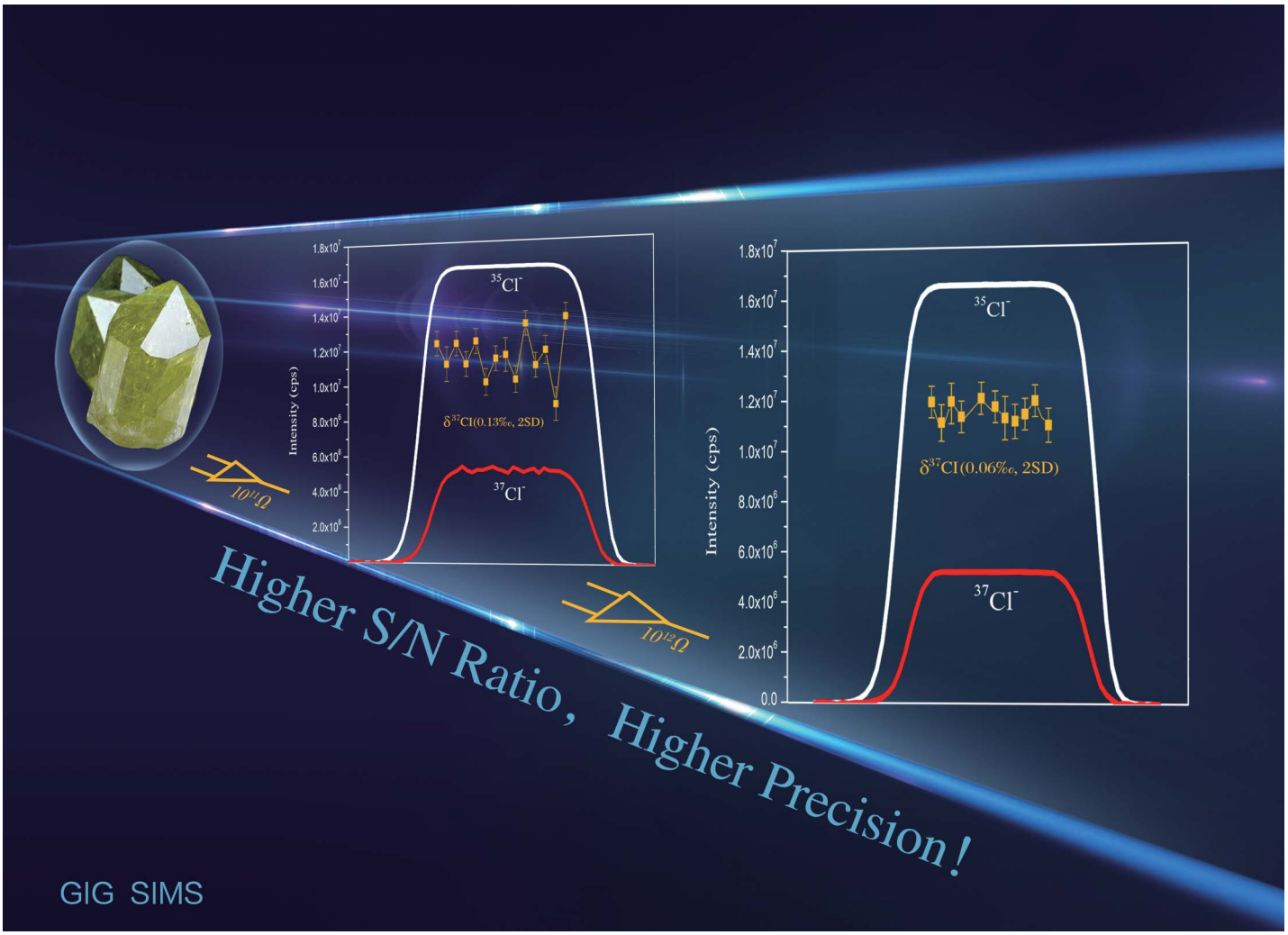

Showcasing research from Professor Xia's laboratory, State Key Laboratory of Isotope Geochemistry, Guangzhou Institute of Geochemistry, Chinese Academy of Sciences, Guangzhou 510640, China.

High-precision apatite $\delta^{37}Cl$ measurement by SIMS with a 10^{12} Ω amplifier Faraday cup

Apatite chlorine isotope analyses on four natural reference materials was conducted, using an ion probe equipped with a 10^{12} Ω FC preamplifier board, which yielded an analytical precision (internal error and reproducibility) that was significantly improved by a factor of two from conventional analytical procedures.

As featured in:

See Qing Yang, Xiao-Ping Xia *et al.*, *J. Anal. At. Spectrom.*, 2022, **37**, 222.

ROYAL SOCIETY OF CHEMISTRY

rsc.li/jaas

Registered charity number: 207890

JAAS

ROYAL SOCIETY OF CHEMISTRY

TECHNICAL NOTE

View Article Online
View Journal | View Issue

Cite this: *J. Anal. At. Spectrom.*, 2022, **37**, 222

High-precision apatite δ^{37}Cl measurement by SIMS with a 10^{12} Ω amplifier Faraday cup†

Zexian Cui, [abc] Qing Yang, *[ab] Xiao-Ping Xia, *[abc] Rui Wang,[d] Magali Bonifacie,[e] Chun-Kit Lai, [f] Wan-Feng Zhang, [abc] Yan-Qiang Zhang[ab] and Jian Xu[ab]

Chlorine is a redox-sensitive and fluid-mobile element, and is involved in many geological processes. Apatite, a ubiquitous accessory mineral in mafic to felsic rocks, is the most-studied mineral in chlorine isotope research due to its abundant structural chlorine [$Ca_5(PO_4)_3$(F, Cl, OH)]. Although a wide δ^{37}Cl range (up to 40‰) has been reported for extraterrestrial samples, the terrestrial apatite δ^{37}Cl range is much narrower (0 ± 0.5‰) and thus high-precision measurement is necessary. However, analytical uncertainties of the published apatite δ^{37}Cl by secondary ion mass spectrometry (SIMS) are generally above 0.20‰ (2SD; especially for Cl-poor (<1 wt%) samples), which are insufficient for most geological studies. To improve the analytical precision, we investigated the performance of a 10^{12} Ω amplifier Faraday cup (FC) for apatite δ^{37}Cl measurement. A SIMS (CAMECA IMS 1280-HR) multi-collector system was adopted, and two movable FCs (L1 and H1, with 10^{11} Ω and 10^{12} Ω resistors respectively) were used to collect ^{35}Cl and ^{37}Cl ions. Four natural apatite reference samples (TUBAF#37, Durango, MGMH#128441A, and Eppawala-AP) with 0.27–1.55 wt% chlorine were analysed. Due to the low background noise of the 10^{12} Ω amplifier FC and the elimination of heterogeneous detector interference between the electron multiplier (EM) and FC, the precision (both single spot internal uncertainty and spot-to-spot reproducibility) is significantly improved. The internal uncertainty and spot-to-spot reproducibility can reach 0.10‰ (2SE) and 0.20‰ (2SD), respectively, for a low-Cl (0.27 wt%) sample, while the best reproducibility (0.06‰, 2SD) is achieved for the Eppawala-AP apatite (1.55 wt% Cl). Compared with published analyses of apatite with similar chlorine contents, the analytical precision has been improved by around a factor of two. Our results on the four apatite standards (with ~1 wt% difference in the Cl content) show a linear correlation between the measured SIMS instrument mass fractionation (IMF) and the chlorine concentration in apatite, which need to be corrected in future analyses. The analytical accuracy is also improved, as deviation of the corrected SIMS values from those of the GS-IRMS analysis is below 0.05‰ for the three analysed reference materials (TUBAF#37, Durango and Eppawala-AP), whilst MGMH#128441A exhibits a large deviation of 0.35‰, possibly due to the poorly-constrained GS-IRMS results. This provides important guiding significance for future chlorine isotope analyses and warrants further investigation.

Received 12th October 2021
Accepted 6th December 2021

DOI: 10.1039/d1ja00347j

rsc.li/jaas

1. Introduction

Chlorine is a volatile and strongly hydrophilic element. It has two stable isotopes (^{35}Cl and ^{37}Cl), with a natural abundance of 75.77% and 24.23%,[1] respectively. Measurement of the Cl concentration and ^{37}Cl/^{35}Cl ratio can be used to trace metasomatic processes in the crust and mantle,[2–9] predict activities of active volcanoes,[10–14] and model planetary formation and evolution.[15–20] The chlorine isotopic composition is expressed in standard delta notation: $\delta^{37}\text{Cl} = [(^{37}\text{Cl}/^{35}\text{Cl}_{\text{sample}})/(^{37}\text{Cl}/^{35}\text{Cl}_{\text{SMOC}}) - 1] \times 1000$, where SMOC = standard mean ocean chloride (0‰).[21] Apatite ($Ca_5(PO_4)_3$(F, Cl, OH)) occurs in many rock types in both differentiated and undifferentiated planetary bodies including the Earth,[22–24] Moon,[18,20,25–27] Mars,[28–30] asteroid 4-Vesta,[17,31,32] and in various achondrites.[33,34]

[a]State Key Laboratory of Isotope Geochemistry, Guangzhou Institute of Geochemistry, Chinese Academy of Sciences, Guangzhou 510640, China. E-mail: qingy@gig.ac.cn; xpxia@gig.ac.cn

[b]CAS Center for Excellence in Deep Earth Science, Guangzhou, 510640, China

[c]Southern Marine Science and Engineering Guangdong Laboratory (Guangzhou), Guangzhou 511458, China

[d]State Key Laboratory of Geological Processes and Mineral Resources, Institute of Earth Sciences, China University (Beijing) of Geosciences, Beijing 10083, China

[e]Institut de Physique du Globe de Paris, CNRS, Université de Paris, Paris F-75005, France

[f]Faculty of Science, Universiti Brunei Darussalam, Gadong BE1410, Brunei Darussalam

† Electronic supplementary information (ESI) available. See DOI: 10.1039/d1ja00347j

Apatite can hold varying amounts of F, Cl, and OH in its crystal structure,[35] thus is ideal for investigating chlorine isotopes. Multiple studies of lunar and martian apatite exhibit a wide δ^{37}Cl range (−6.6 to +40‰),[26,36] yet the δ^{37}Cl range in most terrestrial materials is much narrower (−5 to +5‰),[37] mostly 0 ± 0.5‰.[38] This means that high-precision chlorine isotope measurement is essential for the research of terrestrial materials.

Complex and often overprinting geological processes including crystallisation, overgrowth, and alteration[24,39] may have generated fine, compositionally-heterogeneous domains in apatite grains,[23] which requires highly-sensitive and high-resolution microanalysis techniques such as secondary ion mass spectrometry (SIMS). Moreover, the small volume of the sputtered material makes it ideal for analysing rare samples by SIMS . Layne *et al.*[40] developed a method for glass δ^{37}Cl determination, using a CAMECA IMS 1270 ion probe with a single electron multiplier (EM) as the detector and yielded an analytical reproducibility of 1.5‰ (2SD).[40] Subsequently, the new generation of the large-radius SIMS (CAMECA IMS 1280/1280-HR) was utilised for this purpose, and two Faraday cups (FCs) in the multi-collection mode were used to collect ^{35}Cl and ^{37}Cl signals simultaneously. This greatly improves the reproducibility to 0.5‰ (2SD),[41] and even to 0.04‰ (2SD)[42] for a high-Cl (6 wt%) sample. For most samples (with < 2 wt% Cl), the analytical uncertainty can only reach ∼0.2‰ (2SD).[42,43] This level of analytical uncertainty can meet some isotopic systems with large fractionation (*e.g.*, oxygen and sulfur) but not for chlorine. The main difficulty in obtaining high-quality data for low-Cl samples lies in the conventional procedure of using an FC detector with a 10^{11} or 10^{10} Ω resistor, which has a relatively high background. Bouden *et al.*[44] measured the backgrounds of FCs equipped with 10^{11} and 10^{10} Ω preamplifiers, yielding up to 5000 and 2000 counts per second (cps), respectively, with a poor reproducibility (1SD) of 2600 and 600 cps.[44] Such high-backgrounds are unsuitable for high-quality chlorine isotope analysis for low-Cl samples (*e.g.*, ∼0.27 wt%; ∼4 × 10^6 cps[44]). Because the noise dictates the level of the background, reducing the noise can effectively reduce the background and thus improve the analytical precision.[44,45] Although the EM can resolve the noise problem, it is limited by the EM aging effect and dynamic range (*ca.* 1–2 × 10^6 cps) of the ion counters. The EM aging effect can be controlled by monitoring the drift of the Pulse Height Amplitude (PHA) curve towards lower voltages, and is compensated by increasing the EM voltage,[46] but it still hampers high-precision isotope analysis. A gap remains in the dynamic range between ion counters of the EM and FCs, *i.e.*, from ∼2 × 10^6 cps (maximum of the EM) to ∼2.5 × 10^6 cps (minimum of 10^{11} Ω amplifier). The 10^{12} Ω amplifier boards of CAMECA instruments can reduce the noise and help to fill this gap. According to the Johnson–Nyquist (JN, detector) noise formula, the use of a 10^{12} Ω amplifier (instead of a 10^{11} Ω amplifier) could improve the signal-to-noise ratio (SNR) √10-fold,[44] and has therefore the potential to improve the measurement precision. In the last decade, development on FC preamplifier boards equipped with a 10^{12} Ω resistor (and even a 10^{13} Ω resistor for thermal ionisation mass spectrometry (TIMS) instrument) allows the reduction of JN noise contribution, and thereby extends the lower-range use of FC detectors.[45,47–50] The adoption of 10^{12} Ω amplifier boards for large radius ion microprobes was first performed on SHRIMP instruments,[46] and more recently on CAMECA instruments.[44,51]

In this study, we used a CAMECA IMS 1280-HR with a 10^{12} Ω FC preamplifier board, which reduces the noise of the FC and eliminates the heterogeneous detector interference (between the EM and FC) for apatite Cl isotope analyses, hence improving the analytical precision.

2. Sample description and preparation

In this study, we analysed four natural apatite reference samples (TUBAF#37,[42] Durango,[42] MGMH#128441A,[42] and Eppawala-AP[43]), which have been demonstrated to be homogeneous in chlorine isotopes at the micrometer-level, and were used as standards for previous SIMS chlorine isotope measurement.[42,43]

The internal structure and major element compositions of these apatite minerals were previously obtained by electron probe microanalysis (Table 1).[42,43] No textural or compositional zoning was observed. The green fluorapatite TUBAF#37 contains minor inclusions of pyrite, quartz, calcite, Ca–Mg silicates, Mg–Fe-aluminosilicates, Ba-/Ca-sulfates, and zircon. The chlorine mass fraction of TUBAF#37 varies slightly with the electron beam current (median 0.27 wt% (for 5 nA) and 0.26 wt% (for 40 nA)), and the recommended δ^{37}Cl value is +0.20 ± 0.26‰ (2SD).[42] The yellow/yellowish-green apatite Durango (from the Cerro de Mercado Fe deposit, Mexico) has 0.47 wt% Cl on average. Same fragments of this Durango sample have been used for SIMS δ^{37}Cl measurements, with the recommended δ^{37}Cl value of +0.19 ± 0.12‰ (2SD).[42] The yellow fluorapatite MGMH#128441A has minor inclusions of Fe-oxides, Ca–Mg–Fe–Mn-silicates, and aluminosilicates (some of which may contain minor Cl) and monazite. The chlorine mass fraction of MGMH#128441A is also slightly dependent on the electron beam current (median 0.99 wt% (for 5 nA) and 1.03 wt% (for 40 nA)), and the recommended δ^{37}Cl value is +0.42 ± 0.40‰ (2SD).[42] The apatite Eppawala-AP has on average 1.55 wt% Cl, and its mineral inclusions are mostly carbonates.[43] The recommended δ^{37}Cl value for Eppawala-AP is −0.74 ± 0.15‰ (2SD).[43]

These samples were embedded in random orientations to form a standard epoxy SIMS mount for the analysis. Mineral grains were placed within a 6 mm circle domain in the center in each mount to avoid possible "X–Y effects".[52,53]

3. Instrumentation

We used a CAMECA IMS 1280-HR secondary ion mass spectrometer installed at the SIMS Laboratory of Guangzhou Institute of Geochemistry, Chinese Academy of Sciences (GIGCAS). The instrument is a large-geometry, double-focusing mass spectrometer equipped with both mono- and multi-collector

Table 1 Sample information[b]

Sample	MGMH#128441A	TUBAF#37	Eppawala-AP	Durango
Description	Fluorapatite Colorado, USA	Fluorapatite Bamble, Norway	Fluorapatite Sri Lanka	Fluorapatite Durango, Mexico
δ^{37}Cl ‰	0.42 ± 0.40	0.20 ± 0.26	−0.74 ± 0.15	0.19 ± 0.12
P_2O_5	40.53	41.13	42.36	40.57
SiO_2	0.52	0.34	—[a]	0.44
SO_3	0.11	0.25	0.28	0.32
CaO	53.47	55.29	54.73	54.82
SrO	0.04	0.26	—[a]	0.06
FeO	0.09	—[a]	0.05	—[a]
MnO	0.15	—[a]	0.02	—[a]
Na_2O	0.18	0.03	0.16	0.21
F	2.15	3.22	1.75	3.45
Cl	0.99	0.27	1.55	0.47
Total	98.23	100.79	100.89	100.34
References	42	42	43	42

[a] —, below the detection limit. [b] Major element concentrations quoted in wt%.

systems. The multi-collector system consists of seven motorised detectors, which move along the focal plane to optimise the collection of different masses. In this study, ^{35}Cl and ^{37}Cl ions were collected simultaneously in static mode using two Faraday cups and were amplified by circuits with 10^{11} Ω (in the L1 position) and 10^{12} Ω (in the H1 position) resistance, respectively. A primary Cs^+ beam (~2.0 nA) was accelerated at 10 kV and focused in the Gaussian mode to sputter the samples. A 15 × 15 μm^2 raster is usually applied to the Gaussian primary beam to ensure flat-bottomed pits. A normal-incidence electron gun was used to ensure charge compensation and to maintain the voltage stability. Negative secondary ^{35}Cl and ^{37}Cl ions were extracted and accelerated at a 10 kV potential. The energy slit was set to a 50 eV bandwidth and shifted 5 eV below the maximum transmission. A 4000 μm field aperture, a 400 μm contrast aperture, a 120 μm entrance slit, 600 μm exit slit, and 100x transfer optical magnification were used to guide the secondary ions. The purpose of the transfer optic lenses, apertures, and slit setting was to ensure maximum transmission of secondary ions for a given mass resolution, by minimising secondary beam aberrations before entering the double-focusing mass spectrometer. Gains of the FCs are inter-calibrated at the beginning of each analytical session. The secondary ions were centered in the field aperture and the entrance slit by scanning the peak of ^{35}Cl. The instrument was equipped with an optional nuclear magnetic resonance (NMR) controller, which acts as a long-term magnetic field regulation controller to stabilise the magnetic field. One measurement (4–5 min) typically comprises 60 s pre-analysis sputtering, which used a 25 × 25 μm^2 raster to clean the sample surface and attain stable count rates on detectors, and 24 cycles of data collection.

4. Results

Two SIMS measurement sessions were conducted to check the analytical precision and accuracy, with the results listed in the Appendix table and summarised in Table 2. The mean uncertainty of single analysis for each sample is from 0.03‰ (2SE; Eppawala-AP) to 0.17‰ (2SE; TUBAF#37) (Fig. 1). The

Table 2 Mean SIMS-measured δ^{37}Cl value and IMF for the samples analysed

Sample ID	Session	Number of fragments	Number of analyses	Measured ^{37}Cl/^{35}Cl ratios		SIMS δ^{37}Cl (‰)	2SD[a]	2SD[b]	IMF	2SD
				Range	Mean					
MGMH#128441A	1	15	20	0.320310–0.320360	0.320332	−11.32	0.09	0.12	−11.74	0.41
	2	1	10	0.320483–0.320526	0.320508	−10.78	0.08		−11.21	0.41
		15	15	0.320491–0.320533	0.320503	−10.79	0.07			
TUBAF#37	1	16	21	0.320181–0.320271	0.320220	−11.67	0.18	0.38	−11.87	0.32
	2	1	10	0.320323–0.320413	0.320369	−11.21	0.20		−11.45	0.33
		15	15	0.320287–0.320429	0.320343	−11.29	0.20			
Eppawala-AP	1	17	20	0.320180–0.320212	0.320196	−11.74	0.06	0.13	−11.00	0.16
	2	1	10	0.320386–0.320412	0.320402	−11.11	0.05		−10.37	0.13
		15	15	0.320381–0.320423	0.320396	−11.12	0.07			
Durango	1	16	21	0.320231–0.320312	0.320276	−11.50	0.14	0.24	−11.69	0.18
	2	1	10	0.320378–0.320451	0.320419	−11.05	0.14		−11.22	0.16
		15	15	0.320415–0.320452	0.320435	−11.00	0.07			

[a] and [b] represent the external precision determined by this study and previous studies,[42,43] respectively.

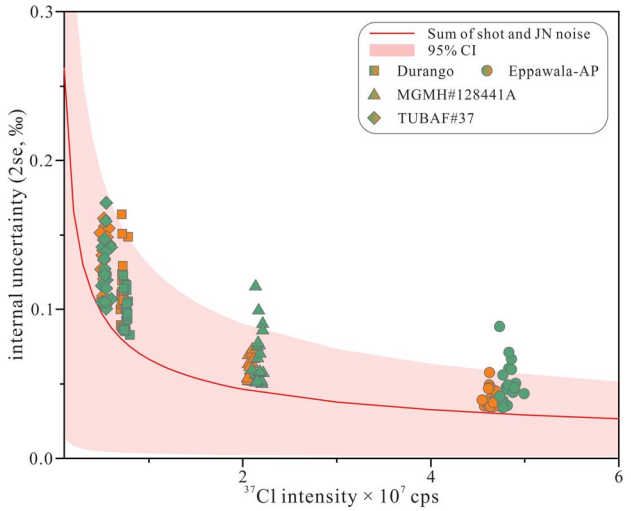

Fig. 1 Theoretical uncertainties and within-spot uncertainties *versus* ^{37}Cl signal intensity (session 1: orange; session 2: green). Red solid line denotes the quadratic sum of shot and JN noise. Pink field denotes 95% confidence limit on the quadratic sum, given the data count times.

instrumental drift was monitored by periodic analyses of the four samples interspersed with each other, and the results show that no offline drift correction is necessary (session 1, Fig. 2A) as the external precision of all samples without drift correction is better than 0.20‰ (2SD; Table 2 and Fig. 2A). In fact, it is even better than the 0.10‰ for Eppawala-AP and MGMH#128441A with > 0.5 wt% Cl. Session 2 exhibits similar internal and external precision to session 1, and there is no significant difference between single- and multi-fragments (Fig. 2B). In this study, the matrix effect was quantified by instrument mass fractionation (IMF) $((\delta^{37}\mathrm{Cl})_{\mathrm{measured}} - (\delta^{37}\mathrm{Cl})_{\mathrm{recommended}})$, whose uncertainty was estimated by: $2\mathrm{SD}_{\mathrm{IMF}} = 2 \times \sqrt{(\mathrm{SD})_{\mathrm{measured}}^{2} + (\mathrm{SD})_{\mathrm{recommended}}^{2}}$. The calculated results are listed in Table 2.

5. Discussion

5.1 Analytical precision

The analytical precision discussed here includes both internal (within a single spot analysis, 2SE) and external (reproducibility) precision of the spot-to-spot results (2SD). The internal precision was calculated from the standard error of the analytical results (of the different cycles in a single spot analysis). It is limited to a minimum value by two simple physical effects: (a) shot (signal) noise and (b) JN noise, which was discussed in detail by Ickert and Stern.[54] The internal precision correlates strongly with counting statistics, which are directly related to

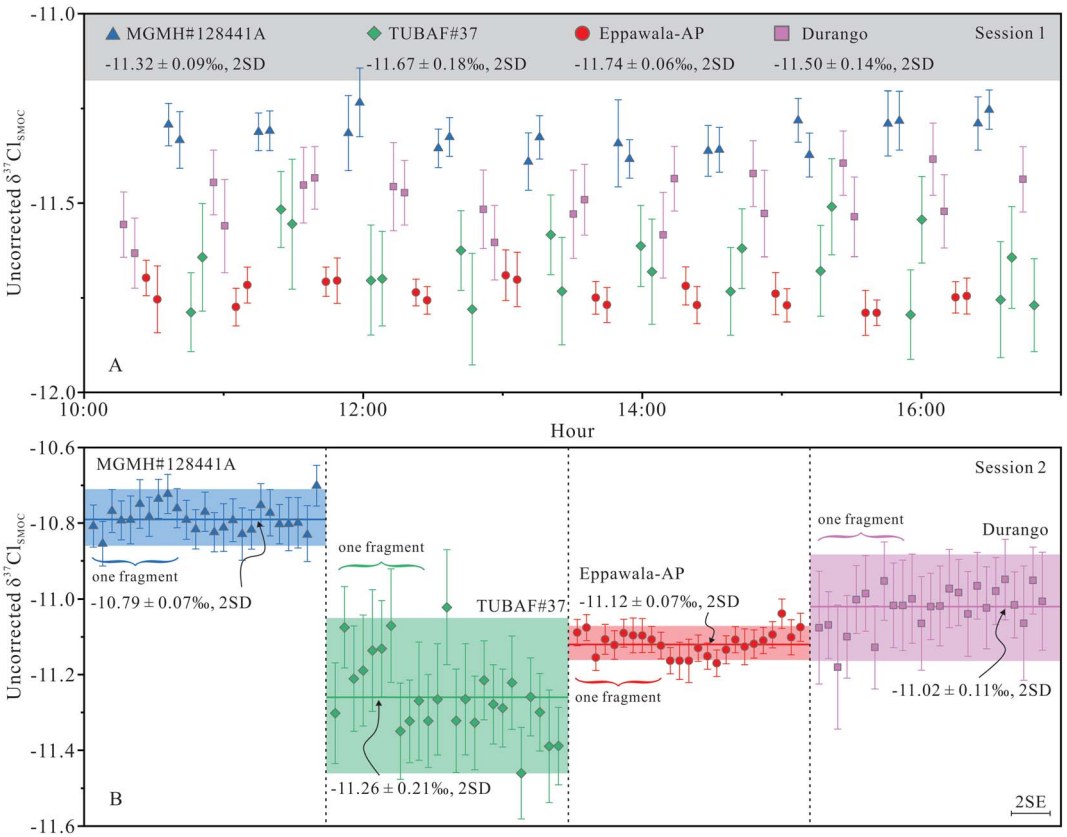

Fig. 2 Reproducibility of measured δ^{37}Cl in this study for the two sessions ((A) Session 1; (B) Session 2). Error bars are ±2SE (standard error). Solid lines denote the external reproducibility (2SD).

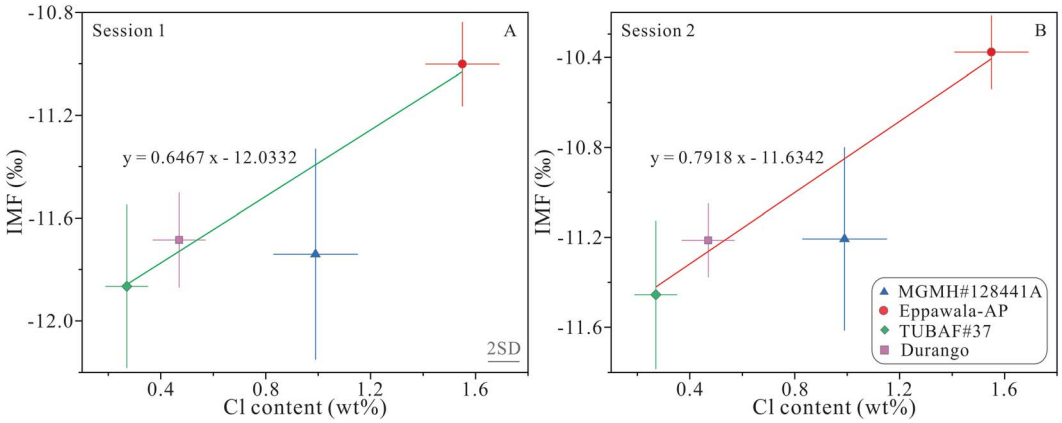

Fig. 3 Variation of the instrumental mass fractionation (IMF) as a function of the Cl content for the two sessions ((A) Session 1; (B) Session 2). The IMF was calculated as the difference between the averaged δ^{37}Cl measured by SIMS and that determined by GS-IRMS. Errors were propagated from both GS-IRMS and SIMS analyses (see text for details). The line and its equation are regressed by using the York fit method with error weighted.

the Cl content, the total counting time, and the primary ion intensity. In this study, the internal precision (2SE) of δ^{37}Cl for all the samples decreases from 0.17 to 0.03‰ with increasing ^{37}Cl intensity, following the theoretical error trend (quadratic sum of shot and JN noise; Fig. 1). The measured and expected values are generally consistent, indicating that on the single-spot scale, two noises are the dominant source of scattering.

The external precision depends on many factors, including the material homogeneity and instrumental stability, which is influenced by environmental variation and the drift of the electron gun and Faraday cups. Previous studies have shown that high external precision in SIMS isotope analysis requires high-quality sample preparation (notably flat surface conditions) and a confined analysis area.[55] The external precision of the two sessions is < 0.21‰ in this study (2SD; Fig. 2), better than that of some previous studies.[42,43] For Eppawala-AP (with ~1.55 wt% Cl), an external precision of 0.06–0.07‰ (2SD) is achieved, representing a major improvement from previous studies (0.13‰ (2SD)[43]). For MGMH#128441A, TUBAF#37, and Durango, the obtained external precision (similar analysis strategy to that of Eppawala-AP) ranges are 0.07–0.09‰ (2SD), 0.18–0.20‰ (2SD), and 0.07–0.14‰ (2SD), respectively (Table 2), which are all significantly improved over previous studies (Table 2). This indicates that the 10^{12} Ω FC preamplifier board can effectively improve the analytical precision, which may be attributed to the reducing noise interference. In addition, it is observed that the external precision (for all the four apatite samples) on a single fragment is the same or worse than that on multi-fragments (session 2; Fig. 2 and Table 2), which further suggests that the chlorine isotopic composition of these reference materials is homogeneous on a microscale of 15 μm size (beam size).

5.2 Matrix effect and accuracy

Matrix effect is a very complex topic, which involves the degree of ionisation of elements during sputtering, and is related to factors such as the mineral composition[56] and crystal orientation.[42,57] It not only acts on concentration measures,[58] but also impacts isotope ratio analysis.[56,59] Previous SIMS apatite isotope analyses showed the impact of matrix effect on the measured chlorine isotope ratios.[41,42] Kusebauch *et al.*[41] found a linear correction between the IMF and Cl mass fraction based on the analyses of natural (Durango) and synthetic chlorapatite. Wudarska *et al.*[42] developed a suite of well-characterised, homogeneous reference apatites covering a wide range of chlorine mass fractions (0.27–6.34 wt%). These authors demonstrated significant matrix effect with different Cl concentrations, and suggested that a calibration curve can be used to correct the effect. The mean IMF value determined for our two Cl content endmembers (TUBAF#37 and Eppawal-AP) differs by 0.87‰ (session 1) or 1.08‰ (session 2), which shows significant matrix effect that should not be overlooked while processing data of unknown samples. Here, the IMF calibration curves were established by comparing the IMF of four reference materials with their Cl content and regressed using the York fit method with error weighting (Fig. 3). To assess the analytical accuracy, all the measurements were treated as unknown and their measured δ^{37}Cl values were corrected using the calibration curves, and the corrected results are listed in Table 3. Although two different calibration curves were

Table 3 Calibrated δ^{37}Cl values

Sample	Session	δ^{37}Cl[a]	2SD	Recommended[b]	2SD
MGMH#128441A	1	0.07	0.09	0.42	0.40
	2	0.06	0.07		
TUBAF#37	1	0.19	0.18	0.20	0.26
	2	0.17	0.20		
Eppawala-Ap	1	−0.71	0.06	−0.74	0.15
	2	−0.71	0.07		
Durango	1	0.23	0.14	0.19	0.12
	2	0.24	0.11		

[a] Data calculated based on the instrument mass fractionation (IMF) *vs.* Cl correlation (details given in the text and Fig. 3). [b] Recommended values are from Wudarska *et al.*[42] and Li *et al.*[43]

obtained in the two sessions, the corrected values are largely the same for each sample. It is noteworthy that the SIMS data corrected for the IMF correspond well with the conventional δ^{37}Cl values (TUBAF#37: 0.19 or 0.17‰ *vs.* 0.20‰;[42] Durango: 0.23 or 0.24‰ *vs.* 0.19‰;[42] and Eppawala-AP: −0.71‰ *vs.* −0.74‰[43]) except for MGMH#128441A (0.07 or 0.06‰ *vs.* 0.42‰). One potential factor contributing to the wide difference of MGMH#128441A is the large δ^{37}Cl variation determined by the three GS-IRMS laboratories (0.23, 0.43, and 0.68‰).[42] We propose that our calibrated value for MGMH#128441A (0.07‰) should be taken as an alternative recommended value, although more work is needed to verify this value between different laboratories using different analytical methods.

6. Conclusion

In this study, analytical performance of the 10^{12} Ω amplifier Faraday cup equipped with a CAMECA IMS 1280-HR has been investigated. Four natural apatite reference samples (TUBAF#37, Durango, MGMH#128441A and Eppawala-AP) with 0.27 to 1.55% chlorine were analysed using the new collector. By reducing the FC noise and eliminating the heterogeneous detector (EM) interference, both the internal and external precision are markedly improved compared with previous studies. The internal and external precision can reach 0.10‰ (2SE) and 0.20‰ (2SD) for a low-Cl (0.27 wt%) sample, and the best external precision can be up to 0.06‰ (2SD) for a high-Cl (1.55 wt%) sample. Compared with previous analyses on the same apatites or on apatites with similar chlorine contents, the analytical precision has been improved by around a factor of two. Through analysing four apatite reference samples with ~1% chlorine content variation, we verified that there is major correlation between the IMF and chlorine content after improving the analytical precision. The analytical accuracy is also improved, and the corrected SIMS values are only 0.01‰ to 0.05‰ drifted from those of the GS-IRMS analysis. This provides important guiding significance for future chlorine isotope analyses and warrants further investigation.

Conflicts of interest

There are no conflicts to declare.

Acknowledgements

This work was jointly supported by the China National Key R & D Program (2018YFA0702600), NSFC (41703004, 42077404), and the China Postdoctoral Science Foundation (2020M672851), and the Key Special Project for Introduced Talents Team of Southern Marine Science and Engineering Guangdong Laboratory (Guangzhou) (GML2019ZD0202). This is contribution No. IS-3110 from GIGCAS.

References

1 T. B. Coplen, J. K. Böhlke, P. D. Bièvre, T. Ding, N. E. Holden, J. A. Hopple, H. R. Krouse, A. Lamberty, H. S. Peiser, K. Revesz, S. E. Rieder, K. J. R. Rosman, E. Roth, P. D. P. Taylor, R. D. Vocke and Y. K. Xiao, *Pure Appl. Chem.*, 2002, **74**, 1987–2017.
2 J. D. Barnes, H. Paulick, Z. D. Sharp, W. Bach and G. Beaudoin, *Lithos*, 2009, **110**, 83–94.
3 J. D. Barnes, Z. D. Sharp and T. P. Fischer, *Geology*, 2008, **36**, 883–886.
4 L. Li, M. Bonifacie, C. Aubaud, O. Crispi, C. Dessert and P. Agrinier, *Earth Planet. Sci. Lett.*, 2015, **413**, 101–110.
5 A. L. Rizzo, A. Caracausi, M. Liotta, A. Paonita, J. D. Barnes, R. A. Corsaro and M. Martelli, *Earth Planet. Sci. Lett.*, 2013, **371–372**, 134–142.
6 Z. D. Sharp, J. D. Barnes, T. P. Fischer and M. Halick, *Geochim. Cosmochim. Acta*, 2010, **74**, 264–273.
7 M. A. Kendrick, V. S. Kamenetsky, D. Phillips and M. Honda, *Geochim. Cosmochim. Acta*, 2012, **81**, 82–93.
8 M. A. Kendrick, C. Hémond, V. S. Kamenetsky, L. Danyushevsky, C. W. Devey, T. Rodemann, M. G. Jackson and M. R. Perfit, *Nat. Geosci.*, 2017, **10**, 222–228.
9 T. E. Johnson, M. Brown, B. J. P. Kaus and J. A. VanTongeren, *Nat. Geosci.*, 2014, **7**, 47–52.
10 A. Aiuppa, D. R. Baker and J. D. Webster, *Chem. Geol.*, 2009, **263**, 1–18.
11 M. Edmonds, *Philos. Trans. R. Soc., A*, 2008, **366**, 4559–4579.
12 M. Edmonds, D. Pyle and C. Oppenheimer, *Earth Planet. Sci. Lett.*, 2001, **186**, 159–173.
13 M. Liotta, A. Paonita, A. Caracausi, M. Martelli, A. Rizzo and R. Favara, *Chem. Geol.*, 2010, **278**, 92–104.
14 C. Oppenheimer, M. Edmonds, P. Francis and M. Burton, *Journal*, 2002, **21**, 621–639.
15 J. R. Darling, L. F. White, T. Kizovski, A. Černok, D. E. Moser, K. T. Tait, J. Dunlop, B. Langelier, J. O. Douglas, X. Zhao, I. A. Franchi and M. Anand, *Geochim. Cosmochim. Acta*, 2021, **293**, 422–437.
16 N. J. Potts, J. J. Barnes, R. Tartèse, I. A. Franchi and M. Anand, *Geochim. Cosmochim. Acta*, 2018, **230**, 46–59.
17 A. R. Sarafian, T. John, J. Roszjar and M. J. Whitehouse, *Earth Planet. Sci. Lett.*, 2017, **459**, 311–319.
18 J. J. Barnes, I. A. Franchi, F. M. McCubbin and M. Anand, *Geochim. Cosmochim. Acta*, 2019, **266**, 144–162.
19 J. W. Boyce, S. A. Kanee, F. M. McCubbin, J. J. Barnes, H. Bricker and A. H. Treiman, *Earth Planet. Sci. Lett.*, 2018, **500**, 205–214.
20 J. W. Boyce, A. H. Treiman, Y. Guan, C. Ma, J. M. Eiler, J. Gross, J. P. Greenwood and E. M. Stolper, *Sci. Adv.*, 2015, **1**, e1500380.
21 R. Kaufmann, A. Long, H. Bentley and S. Davis, *Nature*, 1984, **309**, 338–340.
22 A. Boudreau and A. Simon, *J. Petrol.*, 2007, **48**, 1369–1386.
23 J. W. Boyce and R. L. Hervig, *Geology*, 2008, **36**, 63–66.
24 X. Zhang, F. Guo, B. Zhang, L. Zhao, Y. Wu, G. Wang and M. Alemayehu, *Contrib. Mineral. Petrol.*, 2020, **175**, 35.
25 J. P. Greenwood, S. Itoh, N. Sakamoto, P. Warren, L. Taylor and H. Yurimoto, *Nat. Geosci.*, 2011, **4**, 79–82.
26 A. Gargano, Z. Sharp, C. Shearer, J. I. Simon, A. Halliday and W. Buckley, *Proc. Natl. Acad. Sci.*, 2020, **117**, 23418–23425.

27 Y. Wang, W. Hsu and Y. Guan, *Sci. Rep.*, 2019, **9**, 5727.
28 S. Hu, Y. Lin, M. Anand, I. A. Franchi, X. Zhao, J. Zhang, J. Hao, T. Zhang, W. Yang and H. Changela, *J. Geophys. Res.: Planets*, 2020, **125**, e2020JE006537.
29 J. P. Greenwood, S. Itoh, N. Sakamoto, E. P. Vicenzi and H. Yurimoto, *Geophys. Res. Lett.*, 2008, **35**, 1–5.
30 S. Hu, Y. Lin, J. Zhang, J. Hao, W. Xing, T. Zhang, W. Yang and H. Changela, *Meteorit. Planet. Sci.*, 2019, **54**, 850–879.
31 T. J. Barrett, J. J. Barnes, M. Anand, I. A. Franchi, R. C. Greenwood, B. L. A. Charlier, X. Zhao, F. Moynier and M. M. Grady, *Geochim. Cosmochim. Acta*, 2019, **266**, 582–597.
32 A. Stephant, M. Wadhwa, R. Hervig, M. Bose, X. Zhao, T. J. Barrett, M. Anand and I. A. Franchi, *Geochim. Cosmochim. Acta*, 2021, **297**, 203–219.
33 R. Tartèse, M. Anand and I. A. Franchi, *Geochim. Cosmochim. Acta*, 2019, **266**, 529–543.
34 A. R. Sarafian, E. H. Hauri, F. M. McCubbin, T. J. Lapen, E. L. Berger, S. G. Nielsen, H. R. Marschall, G. A. Gaetani, K. Righter and E. Sarafian, *Philos. Trans. R. Soc., A*, 2017, **375**, 20160209.
35 J. M. Hughes and J. F. Rakovan, *Elements*, 2015, **11**, 165–170.
36 C. K. Shearer, S. Messenger, Z. D. Sharp, P. V. Burger, A. N. Nguyen and F. M. McCubbin, *Geochim. Cosmochim. Acta*, 2018, **234**, 24–36.
37 J. D. Barnes and Z. D. Sharp, *Rev. Mineral. Geochem.*, 2017, **82**, 345–378.
38 Z. D. Sharp, J. D. Barnes, A. J. Brearley, M. Chaussidon, T. P. Fischer and V. S. Kamenetsky, *Nature*, 2007, **446**, 1062–1065.
39 X. Zhang, F. Guo, B. Zhang, L. zhao and G. Wang, *Am. Mineral.*, 2021, **106**, 1679–1689.
40 G. D. Layne, A. Godon, J. D. Webster and W. Bach, *Chem. Geol.*, 2004, **207**, 277–289.
41 C. Kusebauch, T. John, M. J. Whitehouse and A. K. Engvik, *Contrib. Mineral. Petrol.*, 2015, **170**, 34.
42 A. Wudarska, E. Słaby, M. Wiedenbeck, J. D. Barnes, M. Bonifacie, N. C. Sturchio, G. Bardoux, F. Couffignal, J. Glodny, L. Heraty, T. John, C. Kusebauch, S. Mayanna, F. D. H. Wilke and E. Deput, *Geostand. Geoanal. Res.*, 2020, **45**, 121–142.
43 Y. Li, Q.-L. Li, G.-Q. Tang, A. Gargano, Z. Sharp, A. Pitawala, L. Zhao, M.-G. Zhai and X.-H. Li, *At. Spectrosc.*, 2020, **41**, 51–56.
44 N. Bouden, J. Villeneuve, Y. Marrocchi, E. Deloule, E. Füri, A. Gurenko, L. Piani, E. Thomassot, P. Peres and F. Fernandes, *Front. Earth Sci.*, 2021, **8**, 601169.
45 G. Wang, T. Sun and J. Xu, *Rapid Commun. Mass Spectrom.*, 2017, **31**, 1616–1622.
46 T. R. Ireland, N. Schram, P. Holden, P. Lanc, J. Ávila, R. Armstrong, Y. Amelin, A. Latimore, D. Corrigan, S. Clement, J. J. Foster and W. Compston, *Int. J. Mass Spectrom.*, 2014, **359**, 26–37.
47 G. Wang, Y. Zeng, J. Xu and W. Liu, *J. Mass Spectrom.*, 2018, **53**, 455–464.
48 G. Wang, H. Vollstaedt, J. Xu and W. Liu, *Geostand. Geoanal. Res.*, 2019, **43**, 419–433.
49 A. Makishima and E. Nakamura, *J. Anal. At. Spectrom.*, 2010, **25**, 1712.
50 J. M. Koornneef, C. Bouman, J. B. Schwieters and G. R. Davies, *J. Anal. At. Spectrom.*, 2013, **28**, 749.
51 G. Siron, K. Fukuda, M. Kimura and N. T. Kita, *Geochim. Cosmochim. Acta*, 2021, **293**, 103–126.
52 N. T. Kita, T. Ushikubo, B. Fu and J. W. Valley, *Chem. Geol.*, 2009, **264**, 43–57.
53 P. Peres, N. T. Kita, J. W. Valley, F. Fernandes and M. Schuhmacher, *Surf. Interface Anal.*, 2013, **45**, 553–556.
54 R. B. Ickert and R. A. Stern, *Geostand. Geoanal. Res.*, 2013, **37**, 429–448.
55 G.-Q. Tang, X.-H. Li, Q.-L. Li, Y. Liu, X.-X. Ling and Q.-Z. Yin, *J. Anal. At. Spectrom.*, 2015, **30**, 950–956.
56 B.-X. Su, X.-Y. Gu, E. Deloule, H.-F. Zhang, Q.-L. Li, X.-H. Li, N. Vigier, Y.-J. Tang, G.-Q. Tang, Y. Liu, K.-N. Pang, A. Brewer, Q. Mao and Y.-G. Ma, *Geostand. Geoanal. Res.*, 2015, **39**, 357–369.
57 L. White, P. M. Vasconcelos, J. N. Ávila, T. Ubide and T. R. Ireland, *Chem. Geol.*, 2021, **583**, 120461.
58 E. Hauri, J. Wang, J. E. Dixon, P. L. King, C. Mandeville and S. Newman, *Chem. Geol.*, 2002, **183**, 99–114.
59 E. H. Hauri, A. M. Shaw, J. Wang, J. E. Dixon, P. L. King and C. Mandeville, *Chem. Geol.*, 2006, **235**, 352–365.

